



## Shape and structure of (analogue models of) refolded layers

Djordje Grujic<sup>a,\*</sup>, Thomas R. Walter<sup>a,1</sup>, Hansjörg Gärtner<sup>b</sup>

<sup>a</sup>*Geologisches Institut, Albert-Ludwigs-Universität Freiburg, D-79104 Freiburg, Germany*

<sup>b</sup>*Institut für Technische Optik, Universität Stuttgart, D-70569 Stuttgart, Germany*

Received 14 September 2000; revised 28 August 2001; accepted 10 October 2001

### Abstract

The visualisation of the intricate three-dimensional shapes that arise in non-coaxial refolding is an ongoing problem in the study of multiply deformed terrains. Such complex forms also allow space for subjective interpretation of folding sequences. Analogue models offer a solution to the problem of visualisation because the entire surface of a refolded layer can be examined. In addition, analogue models may permit a quantitative geometric study by digitising models in three dimensions. This paper will examine a method for geometric analysis of multiply folded surfaces. We used the results of analogue experiments with paraffin wax where pre-formed single layer folds were deformed to produce *dome-basin* and *dome-crescent-mushroom* interference patterns. The surfaces of buckled layers in these analogue models were digitised to produce virtual models from which accurate attitude measurements of layers and fold hinges were made. To achieve three-dimensional digitising we developed an optical triangulation system based on structured light measurement by the *double-scan* technique. We applied standard analytical tools used by structural geologists for the analysis of the obtained data and we compared experimental structures with natural examples. © 2002 Elsevier Science Ltd. All rights reserved.

*Keywords:* Refolded layers; Multiply deformed terrains; Folding sequences; Analogue models

### 1. Introduction

Besides being aesthetically pleasing, fold interference patterns are perhaps the most widely varying features in deformed rocks. An accurate understanding of their geometry and formation is important because the investigation of superposed folds is an important field technique used to unravel the deformation history. Models based on the assumption of superposed passive-shear folding suggest that the type of fold interference pattern results solely from the orientation of superimposed shortening and extension directions (e.g. displacement field) relative to the initial folds. In passive-shear folding the layer is highly incompetent, and the competence contrast between the layers is low. The layers exert no influence on the process of folding; they simply act as markers that record the deformation. According to the models of passive-shear folding the interference patterns have regular and predictable forms following geometrical rules of superposing a heterogeneous displacement system on an initial fold (e.g. Ramsay, 1962, 1967).

These models, although fairly simplified in terms of natural interference patterns provide an excellent approximation for describing the geometry of fold superposition. Applying these principles, fold interference patterns can be successfully reproduced by mathematical modelling. Small scale features and strain distribution within such numerical models are highly comparable with natural examples (Ramsay and Lisle, 2000), demonstrating the applicability of these models to the natural situations. In nature, however, most refolding occurs under active layer behaviour (i.e. by buckling), and the initial fold might exert a significant influence on the fold interference pattern. To help understand the geometries that result from superposition of two generations of buckle folds numerous analogue-model studies have been performed in the past by various authors (e.g. Ghosh and Ramberg, 1968; Ghosh, 1974; Skjernaa, 1975; Watkinson, 1981; Watkinson and Cobbold, 1981; Odonne and Vialon, 1987; Ghosh et al., 1992; Grujic, 1993). These experiments show that under active layer buckling the type of the interference pattern produced is a strong function of the shape of the initial fold and that superposition of folds results in more complex structures than those formed by passive-shear folding. In the case of active layer behaviour, compatibility problems caused by folding of differently oriented layers cause the formation of accommodation structures (e.g. Ramsay, 1967; Stauffer, 1988).

\* Corresponding author. Current address: Department of Earth Sciences, Dalhousie University, Halifax, Canada B3H 3J5.

*E-mail addresses:* dgrujic@is.dal.ca (D. Grujic), twalter@geomar.de (T. Walter), hgartner@videotron.ca (H. Gärtner).

<sup>1</sup> Current address: GEOMAR, Wischofstr. 1-3, D-24148 Kiel, Germany.

Passive-shear folding is common in glaciers and salt domes where the layers have low competence contrast and the mean competence is low (e.g. Donath and Parker, 1964). Folding and superposed folding by active layer behaviour is, however, more common than the passive layer behaviour. In most layered rocks, even in high-grade terrains, the mechanical instabilities are sufficiently high to trigger active buckling (e.g. Mancktelow and Abbassi, 1992) if one or all directions within the layers are contracted (deformation fields 2 and 3 of Ramsay, 1967, fig. 3-54).

Forms arising by the superposition of folds show a wide spectrum of interference pattern geometry but can be easily divided into four principal types (e.g. Ramsay and Huber, 1987, pp. 475–504): (a) Type 0: *redundant* fold superposition (axial planes and fold hinges of both fold generations are parallel); (b) Type 1 interference: *dome-basin* pattern (initial hinges are folded, the axial planes remain planar); (c) Type 2 interference: *dome-crescent-mushroom* pattern (both initial hinges and axial planes are folded); (d) Type 3 interference: *convergent-divergent* pattern (hinges of two fold generations are coaxial, the initial axial planes are folded). Only Type 1 and 2 interference patterns will be examined here; their complex three-dimensional (3-D) shapes allow room for subjective interpretation of their geometry and deformation history, therefore analogue models may greatly assist their understanding. For example, a combination of these two types of fold interference may suggest more than two phases of folding because of the very complex pattern of axial surfaces and fold hinges (see e.g. Skjerna, 1975; Grujic, 1993; Johns and Mosher, 1996). Likewise, the deformation history of complex interference patterns may be ambiguous if the metamorphic conditions between the two deformation events did not change to produce different mineral assemblages in two fold generations, and if features such as two tectonic fabrics (e.g. cleavages) were lacking (Ramsay and Lisle, 2000, pp. 893–895). Constraining the fold succession is especially difficult in *dome-basin* patterns because they generally do not develop many small-scale structures. Furthermore, highly non-cylindrical folds may result from two phases of folding by progressive unfolding of the first generation of folds (Grujic, 1993, fig. 4) if their axial planes are perpendicular to the principal extension direction of the superposed strain ellipsoid. In such cases, it is difficult to recognise the existence of first-generation folds, and, solely based on layer attitudes, mapping of fold hinges is ambiguous (Grujic, 1993, fig. 10). Finally, if a layer has experienced contraction in all directions (deformation Field 3 of Ramsay, 1967, fig. 3-54), the resulting folds may be very irregular in shape and orientation (e.g. Johns and Mosher, 1996). In nature, with only fragmentary information available, accurate reconstruction of the shape of a non-coaxially refolded layer is almost impossible and, therefore, the inferred sequence of folding events may be erroneous.

To understand fold interference patterns in a quantitative

way, we re-examined paraffin wax models of superposed folds (Grujic, 1993). In those analogue experiments roundness, tightness, and amplitude of the first-folds were varied to investigate their influence on the geometry of the resulting interference patterns. After experimental deformation, the matrix above the competent layer was removed to permit observation of the folded surface. For this study we digitised the surface of such multiply folded layers as well as the moulds used to prepare the corresponding initial folds. Equal-area projections for bedding and fold hinges of initial folds and of the interference patterns were thus generated. These diagrams of structures with known deformation conditions were compared with diagrams of field data, and used to assist interpretation of the related deformation history.

In the following discussion, we will briefly introduce the digitising technique that enabled us to construct orientation diagrams for the analogue models. In combination with photographs and virtual models of the analogue models, we consider these diagrams a helpful tool for interpreting natural interference patterns and for unravelling their deformation history. Namely, diagrams of structures from analogue models with a fully exposed competent layer surface may help to properly read the diagrams of multiply deformed layers. To test this, we analysed a natural example with a large database available and found the best fitting analogue model to it. The key question that will be asked and examined in this paper is essentially how much kinematic information can a field geologist obtain from a study of fold interference patterns.

## 2. Range data acquisition and object reconstruction

In structural geology, detailed and accurate geometric models of structures within the Earth are required before kinematic and dynamic analyses can be conducted. In practice, however, we are restricted to a limited number of attitude measurements of discrete planar and linear structural elements. For regional structures, these data sets are by nature statistically very small. In this analysis of fold interference patterns, we have studied sets of data equivalent to those collected in nature, but have taken advantage of the fully exposed surface of the model to make detailed measurements of the attitude of structural elements. Because measurements of attitudes are difficult and inaccurate due to the small size of the structures, few efforts had been made in the past to study the analogue models from this perspective. Skjerna (1975) presented hand drawn contour lines of refolded layer surfaces and measured the attitudes of layers and fold hinges from contour maps. Since then several automated techniques have been developed to collect range data from 3-D objects. These techniques include laser-beam scanning and techniques based on optical triangulation (e.g. light sectioning, structured light, or stereovision). Range data allow construction of virtual

models, contour maps or cross-sections. More importantly, the attitude of virtual surfaces can be determined with high accuracy and resolution; i.e. measurements of the attitude of structural elements can be taken at each surface point. In this way, one can acquire from analogue models the type of data that are directly comparable with field data.

### 2.1. Double-scan technique

In every optical triangulation method, shadow and occlusion problems are innate deficiencies (Fig. 1); in the case of high unevenness, projection causes shadows, whereas parts of the object are occluded to the camera. On the other hand, the resolution of height depends on the triangulation angle  $\beta$  (Fig. 1), that being the angle between the projector and camera axes (Gärtner et al., 1996). The greater the triangulation angle, the higher the resolution, and yet more areas of the object space lie in shadows or are occluded. In an effort to overcome these problems while maintaining high height-resolution, the *double-scan* technique of structured light measurement (Fig. 2) has been developed at the Institut für Technische Optik, Stuttgart. The method overcomes most of the aforementioned technical problems, is fast and easy to use, and efficiently provides the data needed. This structured light measurement is carried out by the projection of a sequence of progressively narrower parallel binary light stripes onto the measured object (for full explanation see Gärtner et al., 1996). The light patterns projected on a flat surface are straight, and when projected on uneven surfaces appear deformed when viewed from a different angle (Fig. 3). Measurement of the degree of deformation of the stripes provides information regarding topography, and with the angle of projection, the viewing angle and the geometric parameters of the setup, all three co-ordinates of the object point can be calculated (Gärtner et al., 1996). In the optical triangulation technique, a CCD-camera acquires the images of the object illuminated with the structured light pattern. The position of the pixel in the CCD-matrix determines the viewing beam, whereas the intersection point of the viewing beam and the plane of light yields the co-ordinates of a surface point of the object. For each point on the object, which corresponds to a pixel of the CCD-matrix, a string of data ('black and white') produces a final grey value, which is then translated into elevation. Height values are calculated using a triangulation algorithm (Tiziani, 1991). In practice, eight images of a grey-code are projected onto the object to be measured. Each pixel of the CCD-camera acquires, therefore, a sequence of eight intensities of light, one from each of the recordings.

In the *double-scan* setup, a single projector of light patterns is used jointly with an RGB CCD-camera. To compensate for the unavoidable shadows caused by projection from one side, a second pattern is projected at a negative angle to the first beam (Fig. 2). The projector contains a light unit and a liquid crystal display (LCD),

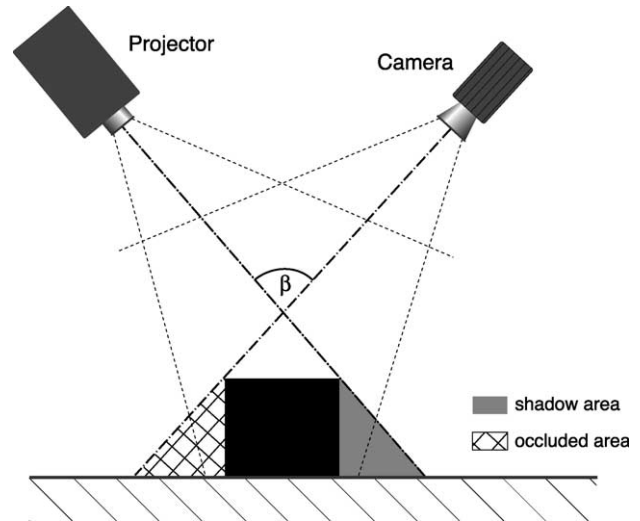


Fig. 1. Shadow and occlusion after Gärtner et al. (1996). To reduce shadow and occluded areas in the object space the triangulation angle  $\beta$  is usually less than  $90^\circ$ . The shadow area is reduced only in one dimension if the triangulation angle decreases. For a large triangulation angle, the resolution is high but the shadow areas are large, and for a small triangulation angle, the shadow areas are small but the resolution is low. Usually a compromise is chosen, depending on the measurement object, so that the shadow areas are not too large and the height resolution is sufficient for the investigation purposes.

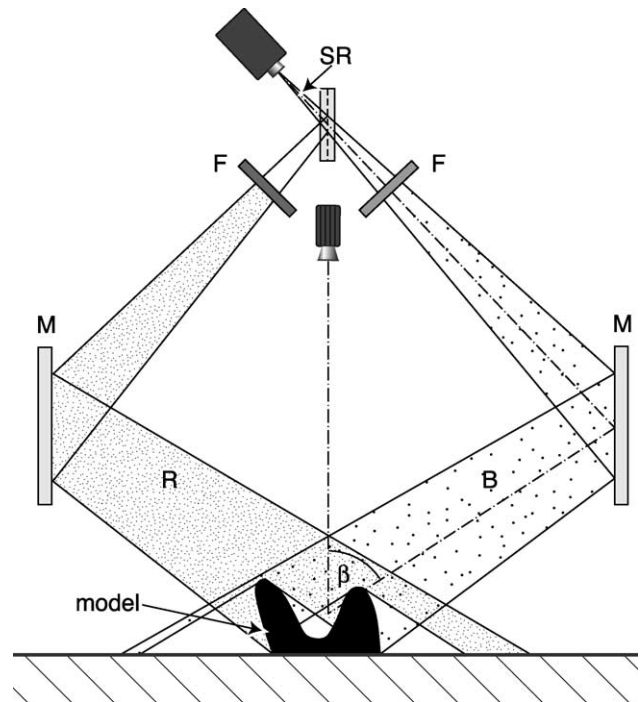


Fig. 2. The principle of the double-scan technique. The structured light (SR) is split into two beams, which are filtered (F) into red (R) and blue (B). The position of the mirrors (M) determines the triangulation angle  $\beta$ . The lower bound for the measurement error  $\Delta z$  for a pixel-based calculation of height values is given by:

$$\Delta z = 1/2 \cdot z_0 / N_L$$

where  $z_0$  is the height of the measurement space, and  $N_L$  the number of projected lines. After Gärtner et al. (1996).

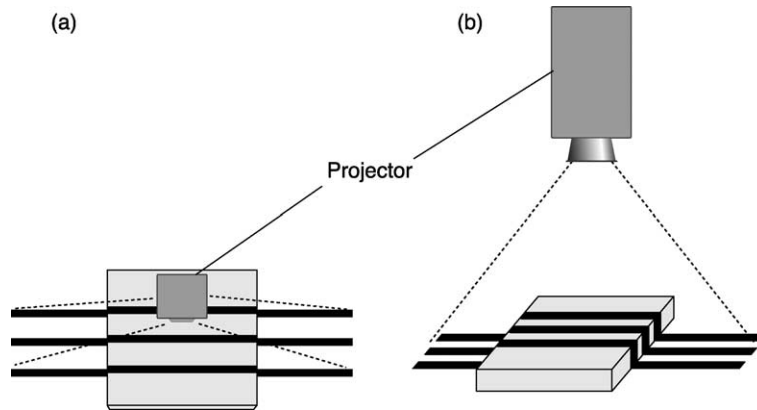


Fig. 3. Regular light pattern projected on uneven objects as viewed from above (a). The light stripes appear deformed if viewed from an oblique angle (b).

which is essential to achieving high accuracy and speed. The LCD produces lines that can be switched on and off at high rate—in our measuring procedure each video frame lasts 40 ms. With a beam-splitter and two mirrors, a second virtual projector is obtained (Fig. 2). To discriminate between the two simultaneously projected light patterns, each beam is assigned a colour (red or blue) using a filter, where the wavelengths of the filters match the spectral characteristics of the red and blue channels of the CCD-camera. As the two channels have wide channel separation (they are divided by the green channel), each channel sees only one illumination pattern. Therefore, only the projection pattern of the corresponding colour is detected. A range data image is calculated from each of the two channels to produce a range map (Gärtner et al., 1996). Since the two measurements are carried out from the same perspective with a single camera, the matching of the two range maps is implicit. Moreover, noise reduction is performed for pixels where two range values can be calculated from the two measurements (averaging the two calculated values reduces the noise). For the object size studied here, the setup offers the greatest horizontal resolution of 0.1 mm, and a height resolution of 0.2 mm. Data acquisition time is approximately 20 s.

## 2.2. Virtual models and diagrams

The database acquired by *double-scan* object digitising consists of Cartesian co-ordinates of object-space points and allows a complex surface to be represented and analysed in three-dimensions. The range map is a complete digital representation of the analysed object. The co-ordinates obtained for each pixel are further processed by 3-DMove® (Silicon Valley). The software creates a virtual object consisting of a mesh of triangles (a.k.a. surface elements) defined by object-points (Gärtner et al., 1996). Typical range maps of refolded models contain ca. 9000 object points (pixels) defining ca. 4000–5000 triangles. Virtual objects can be rotated to a desired view, and contour maps and cross-sections can be produced. Assigning virtual

geographic co-ordinates to the digital model permits the measurement of the attitude of structural features and allows the data to be processed by software for structural analysis (here *Stereoplot* by N.S. Mancktelow). The subroutine for 3-DMove®, used to measure attitude of surface elements (the direction of dip and the angle of dip), STEREO3-D, was written by R. Elsässer, D. Tanner and B. Zehner at the Geologisches Institut, University Freiburg. An additional subroutine for determination of attitude of linear features (e.g. fold hinges) was written by one of our team members (T.W.).

## 3. Refolded layers

### 3.1. Analogue models

The experimental setup and results are only briefly summarised here since detailed descriptions are provided in Grujic (1993). To obtain perfect cylindrical folds without significant perturbations, the initial folds were prepared by hand, carefully wrapping the competent layer made of a paraffin wax around a metal mould with the desired fold shape. The same metal mould was also inserted into the centre of a molten matrix made of a different paraffin wax allowing—upon solidification of the wax—a perfect match of the matrix and the competent layer. This was done in order to achieve reproducible experiments, and a precisely controlled shape of the initial fold, thereby restricting the factors that influence the type and shape of the fold interference. The melting point of the two paraffin waxes differed, allowing a high viscosity contrast of approximately 1:600 at the experimental conditions (e.g. Mancktelow, 1988; Grujic, 1993). The bulk strain superimposed on the fold models had a plane strain–pure shear geometry.

Two sets of experiments were performed with different orientations of initial fold with respect to the principal axes of the imposed strain ellipsoid. This was achieved by placing the initial folds in different orientations within the deformation rig. The orientation of the initial folds is

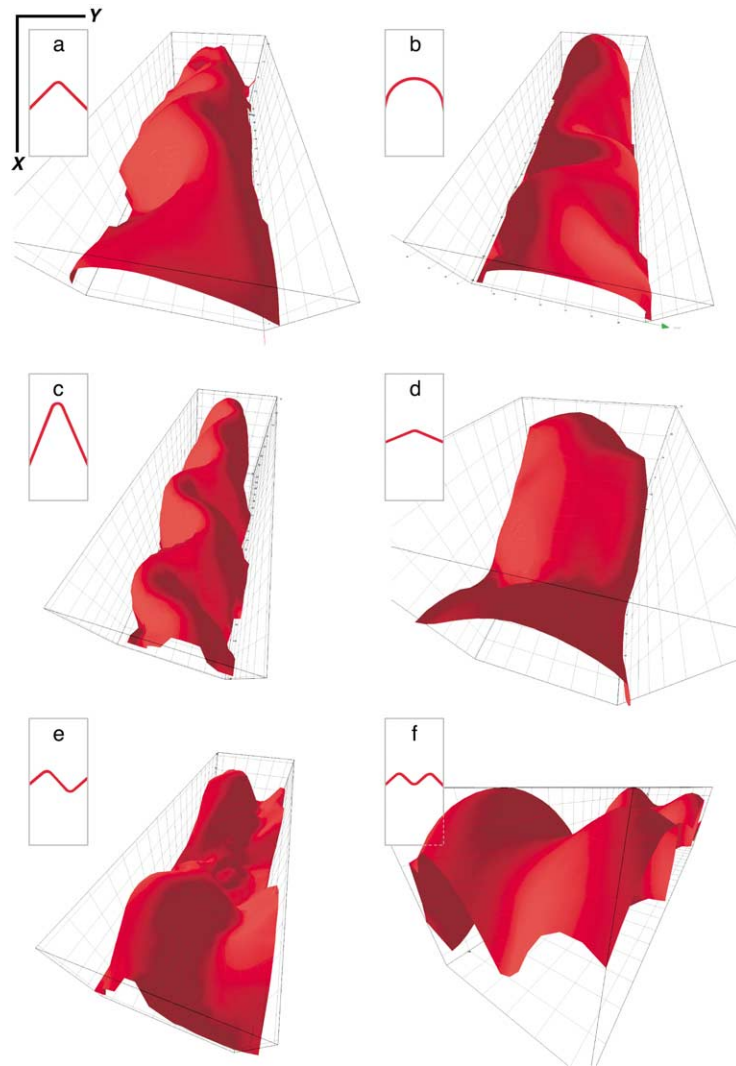


Fig. 4. Perspective projection of models deformed in Type 1 experimental setup (favourable for *dome-basin* interference pattern). In all models the virtual N is pointing to the upper right. The models in sub-figures (a)–(f) are arranged in the same order as in Grujic (1993, fig. 3). The cross-section of the initial-fold as seen in the XY plane of the superimposed strain is given next to the corresponding model.

considered with respect to the external fixed reference frame XYZ, where Z is the direction of maximum shortening, X the principal extension direction, and Y the intermediate extension direction or (in our experimental procedure) direction of no change. Examples of 3-D representations of each analogue model are given in Figs. 4 and 5. In the first set of experiments, the superimposed (i.e. experimental) deformation was oriented such that the direction of maximum shortening Z was parallel to the initial fold hinges, while the initial axial planes were parallel to the XZ plane. Because the principal extension direction X was perpendicular to the first fold hinges, the amplification rate of their buckling was high. In the second set of experiments, the Z direction was equally aligned parallel to the initial fold hinges, but the orientations of the Y and the X extension axes were interchanged, i.e. the initial axial surfaces were parallel to the YZ plane. The first experimental setup was conducive to folding of initial fold hinges within their axial

plane that would remain unfolded. Hence, if the displacements of the second deformation were of heterogeneous simple shear, and if the layering behaved passively, the *dome-basin* interference pattern would have resulted (accordingly 'Type 1 experimental setup'). The second experimental setup was conducive to *dome-crescent-mushroom* interference patterns in which both initial fold hinges and axial planes would become folded (accordingly 'Type 2 experimental setup'). Since the refolding in the analogue experiments occurred by active layer buckling, the initial fold shape exerted a significant influence on the resulting fold interference shape. Consequently, both *dome-basin* and *dome-crescent-mushroom* interference patterns were produced in either experimental setup. Nevertheless, differences between models with the same type of interference pattern, but produced in different experimental setups, are distinctive and, therefore, sufficient to differentiate the two experimental setups. In other words, from the

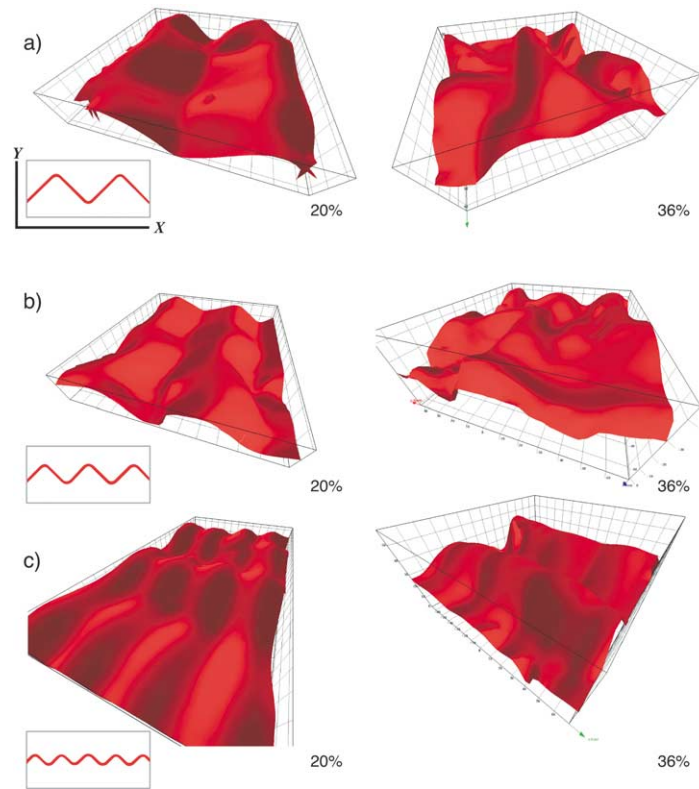


Fig. 5. Perspective projection of models deformed in Type 2 experimental setup (favourable for *dome-crescent-mushroom* interference pattern). In all models the virtual N is pointing to the upper right. The models in sub-figures (a)–(c) are arranged in the same order as in Grujic (1993, fig. 4); all models are seen at 20% (left) and 36% (right) shortening. The cross-section of the initial-fold as seen in the XY plane of the superimposed strain is given next to the corresponding model.

geometry of an interference pattern it is possible to deduce the relative orientation between the initial fold and the principal axes of the superposed strain ellipsoid, both in experiment and nature.

### 3.2. Structural diagrams

Once the deformed models and their respective initial folds were digitised and their virtual models constructed, the attitude of the layer surface ( $S_0$ ), the initial ( $L_1$ ) and the second phase fold hinges ( $L_2$ ) were measured. For the customary representation in the equal-area diagrams (in following, diagrams), it was assumed that for all of the experiments the  $L_1$  were initially horizontal, and their axial planes ( $S_1$ ) vertical, both N–S trending. In diagrams showing data from models deformed in Type 1 experimental setup, the geometrical relationships imply that the direction of maximum shortening Z and the intermediate strain axis Y were horizontal, the former N–S trending, the latter E–W trending. The principal extension direction X was vertical and, therefore, it is projected in the centre of diagrams. In diagrams representing data from models deformed in Type 2 experimental setups, the initial folds and the direction of maximum shortening Z had the same orientation as in the Type 1 experimental setup, while the X and Y axes were interchanged.

In the Type 1 experimental setup, initial folds with six different stiles were deformed by 36% bulk shortening parallel to fold hinges. Bluntness, tightness, and amplitude were varied to investigate the influence of first-fold geometry on the interference patterns. The shape of the initial fold in the cross-section is given next to the corresponding model in Fig. 4. Deformation of fold models in this experimental setup resulted in pronounced interference structures. In models that produced *dome-crescent-mushroom* interference patterns (Fig. 6a and b), the second phase fold hinges are clustered in two maxima because they develop in the limbs of the initial folds (see discussion in Ramsay, 1967, pp. 538–551). The two discrete maxima of bedding-normals of the initially perfectly cylindrical folds are re-distributed along two  $\pi$ -circles ( $\pi$ -circle is a great circle locus defined by the perpendiculars to various surfaces). These  $\pi$ -circles intersect approximately at the initial orientation of the first fold axis (i.e. horizontal, N–S striking). The poles to the  $\pi$ -circles coincide with the maxima of the second-generation fold hinges, which developed in the corresponding limb of the first-generation fold. Where the hinges of the initial folds were broad giving an initial distribution of bedding surfaces ( $S_0$ ) in a partial great circle, the  $\pi$ -circle is preserved after the second deformation. This is most pronounced in rounded and very tight folds (Fig. 4b and c, and the corresponding Fig. 6b and c).

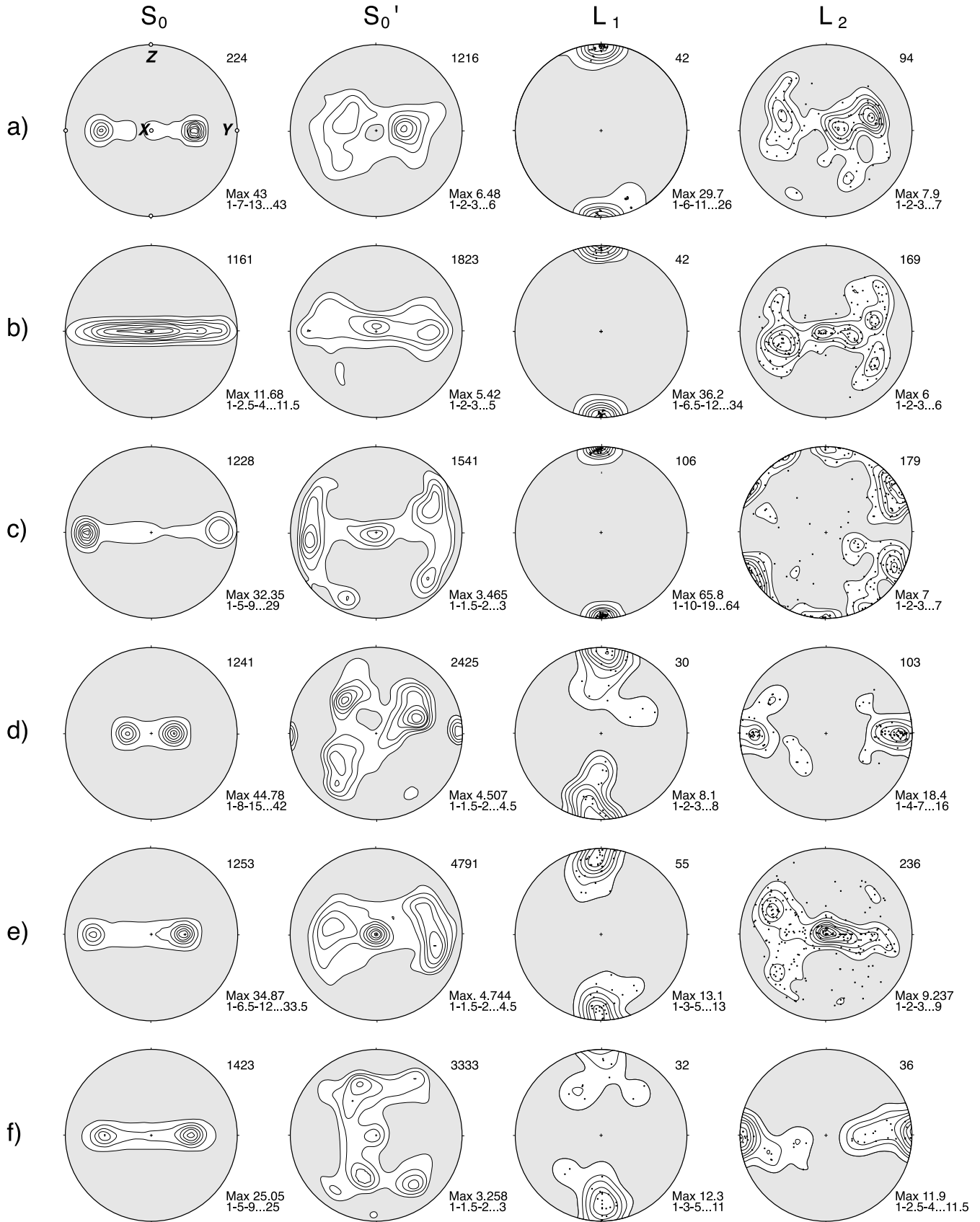


Fig. 6. Diagrams of models given in Fig. 4.  $S_0$ : bedding poles in the initial fold;  $S_0'$ : bedding poles after the second deformation;  $L_1$ : initial-fold hinges after the second deformation;  $L_2$ : second phase fold hinges. Equal area lower hemisphere plot, contoured at times uniform. The diagrams in sub-figures (a)–(f) are arranged in the same order as the corresponding models in Fig. 4. The orientation of the principal axes of the superimposed strain is shown in the first diagram.

The sideways folding of initial hinges increased the hinge area resulting in a new maximum in the first  $\pi$ -circle. The initial fold hinges are scattered around their initial position within a great circle representing the initial fold envelope. The angle of scatter in orientation of the fold hinges is proxy to the interlimb angle of the second phase fold. The deformed  $F_1$  fold hinges are not the initial ones, i.e. these structures are no longer defined by the same material points as before the superimposed deformation. Due to strain compatibility in two opposite-dipping sets of limbs, the initial fold hinges migrate through the material points (e.g. Ghosh et al., 1992; Grujic, 1993). This effect is indicated by the position of the grid-lines that were formerly parallel to the initial fold hinges (e.g. Grujic, 1993, figs. 3 and 4). Hinge migration due to Type 2 interference is intensified by increasing interlimb angle and by increasing bluntness of the initial folds. In natural *dome-crescent-mushroom* interference patterns, the initial fold hinges are, therefore, not parallel to the related material lineations (i.e. intersection, mineral or stretching lineation). The cleavage seen in such folds is a *transected* cleavage, the sense of crosscut relationship changes across the second phase fold hinges (Grujic, 1993, figs. 3a–e and 13). In these cases, the lineations are generally less folded and have smaller scatter around the initial attitude than the fold hinges. In nature, this effect may be difficult to fully document because both material lineations and fold hinges have to be well exposed, and, in the orientation diagrams, the scatter in orientation of these structures may conceal a small intersection angle.

In the elementary *dome-basin* interference pattern (Figs. 4f and 6f), the poles to layering—initially in a  $\pi$ -circle with two distinct maxima—scatter around a  $\pi$ -circle, which is parallel to the superposed XZ plane. The initial fold hinges are scattered in the initial axial plane where the degree of scattering is a proxy for the interlimb angle of the second phase fold. The orientation of the second phase fold hinges is determined by the attitude of the initial fold limbs. However, due to a high degree of roundness in all directions of *dome-basin* forms, hinges are difficult to define precisely even in virtual models. This uncertainty results in additional scatter of the attitudes of both initial and second phase fold hinges.

In the Type 2 experimental setup, models with three stiles of the initial folds were deformed, each in two separate experiments: the first until 20%, the second until 36% bulk shortening parallel to the fold hinges. Two-stage deformation, together with the initial folds, allowed an insight into the evolution of interference structures. Two initial fold shapes resulted in *dome-crescent-mushroom* interference pattern (Fig. 7a and b). The two initial bedding maxima approach each other, reflecting a progressive unfolding of the initial folds because the superimposed stretching direction is perpendicular to the initial axial planes. At higher strain, the two maxima merge in a single elongated maximum, a partial  $\pi$ -circle reflecting only the second phase folds. The initial fold hinges are distributed in

a manner similar to the Type 1 experimental setup, but have progressively higher scatter. The second phase fold hinges are perpendicular to the partial  $\pi$ -circle and have a high scatter. In the models that produced *dome-basin* interference patterns (Fig. 7c), the poles to bedding surfaces behave in the same manner as in the *dome-crescent-mushroom* interference pattern: the two initial maxima merge and evolve in an elongated maximum. The initial fold hinges are refolded within their axial surface, and the second phase fold hinges are perpendicular to the second  $\pi$ -circle. Both generations of fold hinges show higher clustering than in the *dome-crescent-mushroom* interference pattern.

### 3.3. What can analogue models teach us?

Numerous analogue models on superposed folding have demonstrated that the major factor in determining fold interference patterns is the shape of the initial folds and to a lesser extent the orientation of the principal axes of stress or strain of the superimposed deformation. Question may be than asked: can the interference pattern a priori indicate the kinematics of deformation? As proposed by superposed passive-shear folding, the orientation of the second-generation slip direction—usually labelled as  $a_2$ —is parallel to the second phase axial plane and perpendicular to the second phase fold hinge (Ramsay, 1967). Considerable care is, however, required in inferring the orientation of the  $a_2$  in interference patterns produced by active layer buckling. From the study of the analogue experiments, we are of a firm opinion that the analysis following below is applicable to the natural situations as well. In *dome-basin* forms, the  $a_2$  is parallel to the X-direction ( $e_1$  principal finite strain) in the Type 1 experimental setup, and it is parallel to the Y direction ( $e_2$  principal finite strain) in the Type 2 experimental setup. In *dome-crescent-mushroom* forms, the  $a_2$  is parallel to the Y-direction ( $e_2$  principal finite strain) in the Type 1 experimental setup, and it is parallel to the X direction ( $e_1$  principal finite strain) in the Type 2 experimental setup. There is, furthermore, a local  $a_2$  in each limb of the first-generation fold (see discussion in Ramsay, 1967, pp. 538–551). These local slip directions are perpendicular to the fold hinge of second generation and parallel to its axial surface. Both the local and bulk  $a_2$  are located in the plane defined by the two maxima of the second-generation fold hinges. Common for both types of interference patterns, however, is that the orientation of the bulk  $a_2$  is defined by the intersection of great circles of the first and second-generation fold hinges, respectively.

The type of interference pattern and the way it develops (either strengthening or weakening) indicates the approximate orientation between the initial folds and the axes of the imposed strain. In Type 1 experimental setup, the principal extension direction X is parallel to the axial planes of both fold generations and it is perpendicular to the respective fold axes. As a result, the initial folds are passively amplified and the amplification rate of the second phase folds is high. This

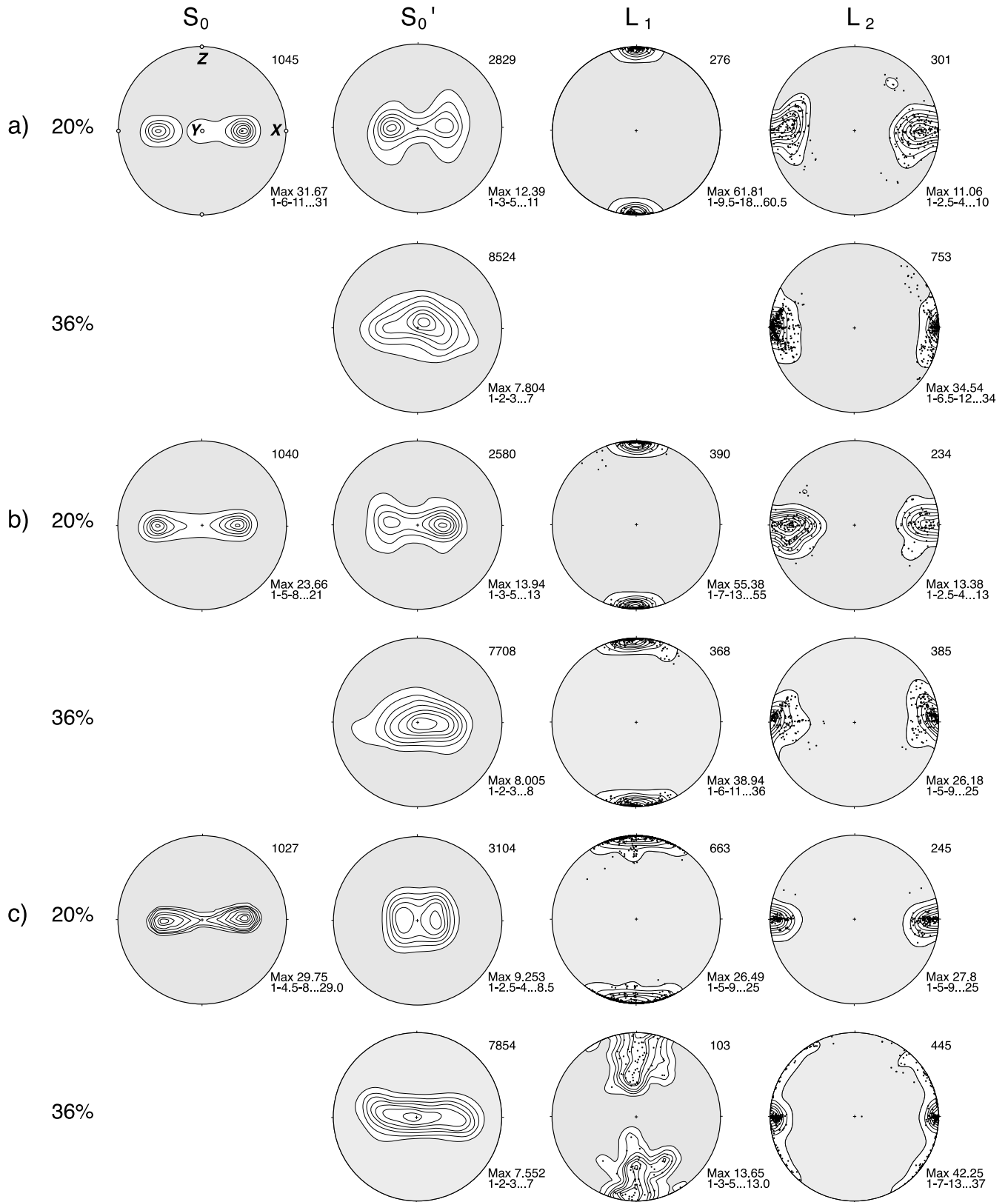


Fig. 7. Diagrams of models given in Fig. 5.  $S_0$ : bedding poles in the initial fold;  $S_0'$ : bedding poles after the second deformation;  $L_1$ : initial-fold hinges after the second deformation;  $L_2$ : second phase fold hinges. Equal area lower hemisphere plot, contoured at times uniform. The diagrams in sub-figures (a)–(f) are arranged in the same order as the corresponding models in Fig. 5. The orientation of the principal axes of the superimposed strain is shown in the first diagram.

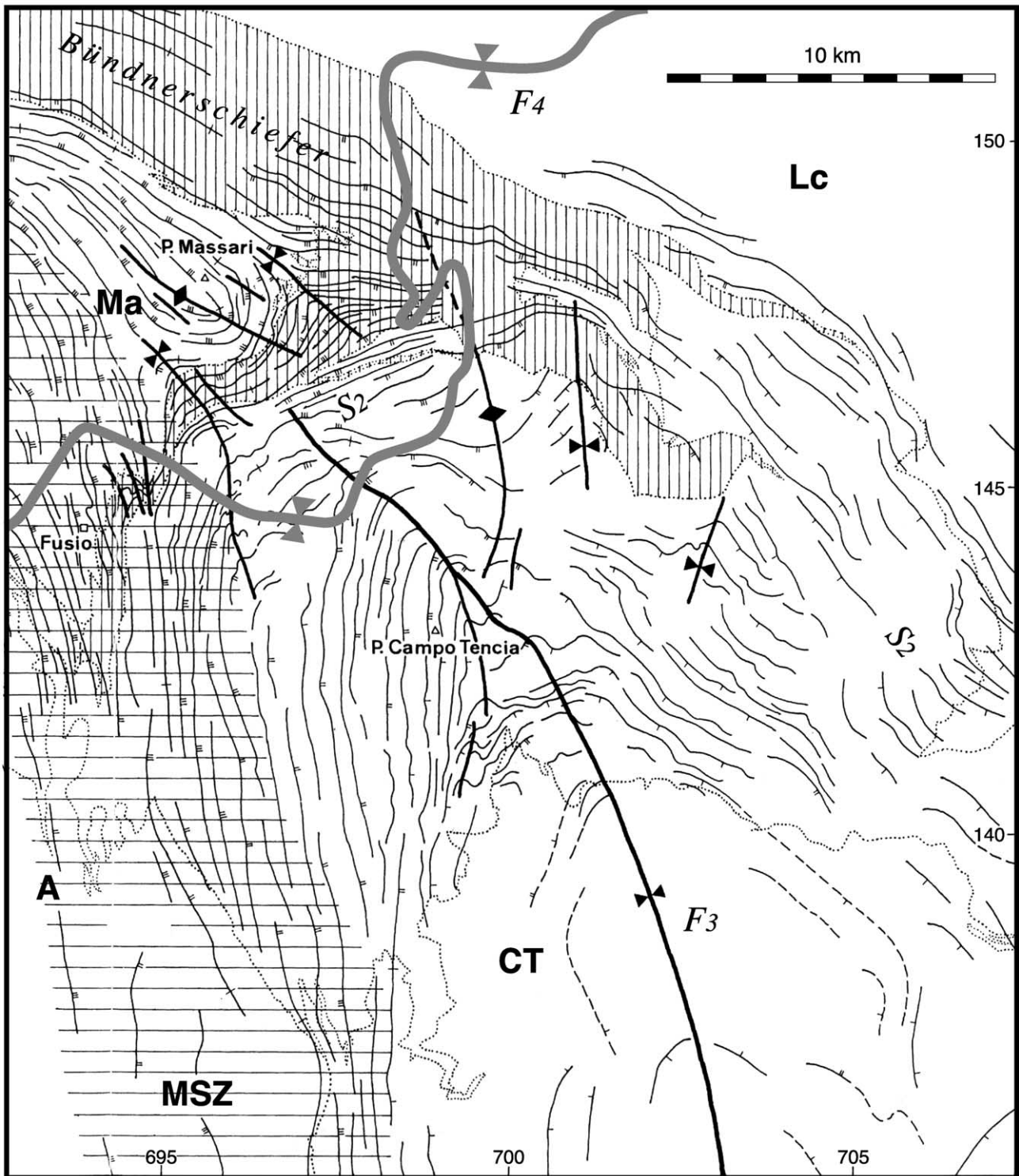


Fig. 8. Structural map of Campolungo area (Ticino, Switzerland) after Grujic and Mancktelow (1996). Shown are the trend of the main regional schistosity,  $S_2$  and axial traces of the main third ( $F_3$ ) and fourth ( $F_4$ ) phase folds. Tectonic units (separated by dotted line), from structurally lower to upper: Lc: Lucomagno Nappe; CT: Campo Tencia-Simano Nappe; A: Antigorio Nappe; Ma: Maggia Nappe. Vertical hatched is Bündnerschiefer, the Mesozoic cover sediments. Horizontal hatched is the Maggia Steep Zone (MSZ), which is a N-S-trending zone of steeply E-dipping main schistosity (interpreted by Grujic and Mancktelow (1995) as the western limb of the third phase synform). Two synforms of third and fourth generation meet in this area to produce a complex basin type interference pattern. Third phase axial plane is approximately vertical in the S and changes to a steep NE dip in the N. The fourth generation axial plane dips shallowly to the N-NW, which results in a complex shape of its trace due to the mountainous area.

results in pronounced interference patterns of both *dome-basin* and *dome-crescent-mushroom* forms. In the Type 2 experimental setup, transient structures arise because the initial folds unfold and the amplification rate of the second phase folds is very low. This occurs because the envelope of the folding layer is parallel to the  $XZ$  plane of the imposed strain (e.g. Fletcher, 1991; Grujic and Mancktelow, 1995, fig. 9). At high strains during the second folding phase no pronounced interference patterns resulted, but rather only gentle, non-cylindrical folds with hinges parallel to the stretching direction of the superimposed strain. In such situations it is difficult to distinguish fold generations only from the topology of the folded layer—the overall geometry may resemble single phase, non-cylindrical folds. These differences between interference forms produced in different orientation of the initial folds to the imposed strain ellipsoid, are clearly reflected in diagrams of the resulting interference structures.

#### 4. A natural example

We compare the experimental data with data from a kilometre-scale fold interference structure in the Campolungo area of the Central Alps (Switzerland), where five generations of alpine folds are present (Huber et al., 1980; Grujic and Mancktelow, 1996; Steck, 1998). First generation structures are largely obliterated by second phase structures, which developed during the thermal peak of metamorphism to produce the dominant schistosity  $S_2$ . This penetrative schistosity is axial planar to recumbent, tight folds. The third phase structures developed obliquely to the trend of earlier structures and to the Penninic zone as a whole. These open, upright folds had developed a new crenulation, axial planar cleavage. Fourth phase folds represent the backfolds of the *Northern Steep Zone* (Milnes, 1974). Fifth phase structures are coaxial with  $F_4$  and only locally developed within the steep zone. These open non-cylindrical structures did not significantly alter the attitude of the main schistosity. First-order folds of the third and fourth generation meet in the Campolungo area producing a pronounced interference pattern outlined by the lithological boundaries and dominant schistosity (Fig. 8).

In the following section, we compare the orientation of natural structures to equivalent experimental structural elements in search of the best matching experimental model to use as an aid for interpretation of the natural example. We compare the attitude of the dominant schistosity  $S_2$  folded by the third and fourth generation folds with the attitude of the competent layer in the analogue experiments. Likewise, we compare the attitude of the third and fourth phase Alpine fold hinges with the first and second phase experimental fold hinges, respectively. For the following analysis, it was assumed that the main schistosity  $S_2$  was near planar before the onset of the third deformation (this is correct within a scatter of  $10^\circ$ ), i.e.  $S_2$  featured as the

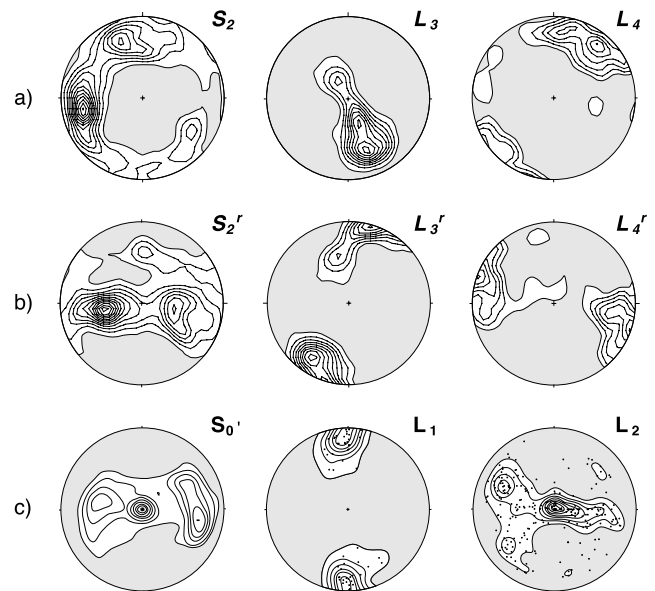


Fig. 9. Diagrams of structures in Campolungo region:  $S_2$ —1356 data; contoured at 0.5, 1, 1.5...6 times uniform;  $L_3$ —379 data, contoured at 1, 2, 3...9 times uniform;  $L_4$ —55 data, contoured at 1, 2, 3...7 times uniform. (a) Data plotted in the geographic co-ordinates. (b) Data rotated into approximately symmetric position within the diagram, equivalent to the projection of the data from analogue models. Rotation parameters were same for all three datasets. (c) For comparison the diagrams from Fig. 6e for the model shown in Fig. 4e.

reference surface. The third generation folds  $F_3$  deformed the  $S_2$  to produce the *initial* folds, which were consecutively refolded by the  $F_4$ —the two together giving rise to the conspicuous regional interference pattern. In Fig. 9a we plot  $S_2$ ,  $L_3$ , and  $L_4$  in geographic co-ordinates. To facilitate the comparison of the natural structures with the corresponding experimental structures, the natural data were rotated into a symmetrical position within the diagram ( $S_2'$ ,  $L_3'$ , and  $L_4'$ ), equivalent to the orientation of the experimental data (Fig. 9b). The same rotation angles were applied for all three sets of data. In this way we can compare experimental with natural structures,  $S_0'$  to  $S_2'$ ,  $L_1$  to  $L_3'$ , and  $L_2$  to  $L_4'$  (Fig. 9b and c). After the rotation the main schistosity is distributed in a complex manner: the  $\pi$ -poles form two  $\pi$ -circles, one complete with two maxima, the second partial and much weaker with a single maximum. The two  $\pi$ -circles are related to distribution of the schistosity in two limbs of the major  $F_4$  synform. The difference in the strength of maxima, e.g. in the number of data, is probably related to different sampling in the limbs of the synform. Fewer field measurements from the steep northern limb of the synform are due to its smaller outcrop surface relative to the southern, flat limb. The third phase fold hinges,  $L_3$  are distributed in a great circle approximately perpendicular to both  $\pi$ -circles defined by the main schistosity. The fourth phase fold hinges,  $L_4$  are scattered in a great circle perpendicular to the  $L_3$ -great circle.

The best match for three diagrams from Campolungo are the equivalent diagrams for the model deformed in Type 1

experimental setup, resulting in a combination of *dome-basin* and *dome-crescent-mushroom* interference patterns with the former pattern dominant (Figs. 6e and 9c). That is, the experiment in Fig. 4e shows similarities to the pattern of superposed folding between first order  $F_3$  and  $F_4$  synforms in the Central Alps. Major features of the topology of the corresponding diagrams are: (i) the poles to reference surfaces ( $S'_0$  and  $S'_2$ ) show tendency for distribution in two inclined, N–S trending  $\pi$ -circles and in a small circle around a horizontal N–S axis. In more general terms, the two  $\pi$ -circles intersect at the locus of the initial fold axis; (ii) the initial fold hinges ( $L_1$  and  $L'_3$ ) are in a partial great circle striking N–S with a maximum near the initial orientation of the first-generation fold hinge; (iii) the superposed fold hinges ( $L_2$  and  $L'_4$ ) scatter around the great circle striking E–W. The experimental data presented in Fig. 6e provide the most reasonable match to the data from the natural example although similarities to the diagrams in sub-Figs. 6b and 7b can be also found. The major deviation from the natural example in the two latter cases is that their first-generation fold hinges are distributed in a horizontal plane (the envelope to the initial fold); e.g. in the corresponding experimental models the *dome-crescent-mushroom* interference pattern is dominant. To select the most reasonably matching experimental model it was necessary to compare the diagrams for all the structural elements, and take into account how pronounced is the interference structure with respect to the estimated magnitude of the bulk finite strain.

The analogue model shown in Fig. 4e would be therefore the 'type' shape of the interference pattern between the major folds of the third and fourth deformation phase, as depicted by the main schistosity. The complete image is, however, much more complex because the lithological boundaries are not parallel to the  $S_2$  (the  $S_2$  is axial planar cleavage to tight second phase folds; Huber et al., 1980). Nevertheless, because we know the deformation history of the analogue experiment we can use that knowledge to unfold the natural interference pattern and to estimate the initial attitude of the former fold generation, the  $F_3$  synform. In this way, we may infer the initial attitude of the third phase axial plane (sub-vertical to steeply E–NE-dipping) and fold axis (gently SE–SSE-plunging). Since the natural interference pattern resembles the pattern produced in Type 1 experimental setup one could further argue that the most likely orientation of the principal strain  $e_3$  during the fourth deformation phase was sub-parallel to the  $F_3$  axes. In case of a likely non-rotational strain history during this deformational phase (based on lack of related shear zones and kinematic indicators showing non-coaxial strain), this may have been also the main tectonic shortening direction  $Z_4$ . Similarly we may infer that the principal tectonic extension direction  $X_4$  was parallel to the axial surfaces of both fold generations and was perpendicular to the respective fold axes, i.e. steeply NNW-plunging. These observations are compatible with the orientation of the  $F_4$  axial planes. The

combination of *dome-crescent-mushroom* with dominant *dome-basin* interference pattern in the Campolungo area is the result of the particular shape of  $F_3$  folds. If the  $F_3$  folds were tighter, with higher amplitude and narrower hinges, the *dome-crescent-mushroom* interference pattern would dominate (as it is the case in smaller scale folds in schists). Conversely, if the  $F_3$  folds were less pronounced and more rounded, only the *dome-basin* interference pattern would be discernible (this is indeed the dominant interference pattern of smaller scale folds in marbles). A similar (though more speculative) effect on the interference pattern would provide the rheology of the rocks during  $F_4$ . If the mean competence of the rocks was higher, the dominant interference pattern would be *dome-crescent-mushroom*; if the mean competence was lower, the dominant interference pattern would be *dome-basin*.

## 5. Conclusions

The detailed and careful study of attitudes of layers and fold hinges provides information of approximate initial fold shape and attitude. In the case of *dome-crescent-mushroom* interference, the poles to layering are distributed in three  $\pi$ -circles. One represents the initial fold; two are related to the second folding event. The two latter  $\pi$ -circles cross at the locus of the initial fold axis and intersect the first  $\pi$ -circle at the locus of the initial fold layering maxima. The initial fold hinges are scattered in a plane that is the envelope of the initial fold. In *dome-basin* interference pattern, poles to bedding cluster in two  $\pi$ -circles with approximately four maxima. These maxima describe a cone (small circle in a diagram) around the superimposed stretching direction,  $a_2$ . The intersection of two  $\pi$ -circles is at the locus of the initial fold axis. If sufficient measurements are made, it is, therefore, possible to distinguish between first and second phase data on the diagrams. For *dome-basin* interference patterns, such differentiation is usually impracticable in the absence of fabric elements (e.g. cleavage) developed under different metamorphic conditions.

Equal-area diagrams of bedding and fold hinges from interference patterns arising by the superposition of shear folds on pre-existing folds have regular and predictable patterns of data distribution. Because the 3-D forms arising by superposition of buckle folds on pre-existing folds are complex and irregular the scatter of data is high. This scatter conceals the details of data distribution, however, major elements of diagram topology (e.g.  $\pi$ -circles, great circles, small circles, and their mutual intersections) can be reliably identified by statistical methods of data analysis. These outlines of orientation of structural elements can greatly assist in the proper identification of the 3-D form of the fold interference.

The shape of an analogue model can be successfully used as the template of natural interference patterns although the

natural structures may be more complex. In cores of orogens the rocks have often undergone several folding phases and the initial planar structures might be strongly transposed making the task of unravelling the earliest structures even more arduous. In multiply refolded areas, therefore, the dominant planar fabric ought to be analysed first, then stepwise the progressively older tectonic surfaces (in the presented example the axial planes of the first phase folds,  $S_1$ ) and finally the lithological boundaries. The latter are the surfaces that we usually draw on the cross-sections, which is a stubborn task in some multiply deformed areas (see the discussion in Hobbs et al., 1976, pp. 373–379).

Careful field analyses of fold interference structures, coupled with the laboratory techniques, deliver information about a deformation history. These techniques must be applied with precaution in regional studies because of important limitations, such as: multiple solutions, small sample size for natural examples, much more complex forms in nature, variable interference patterns in different lithologies, strong transposition of the lithological boundaries by tectonic foliation. We believe, nevertheless, that the 3-D renderings of fold interference structures can be a useful tool for field geologists. For example, this type of structural template may be helpful for the reconstruction of the 3-D shape of large-scale natural fold interference structures. What is more important, however, is the potential to extend the geometric analysis of fold interference patterns beyond the trivial identification of fold generations, since the interference patterns may also provide kinematic information about the deformation history. As it has been demonstrated by Ramsay and Lisle (2000), if adequate strain markers are present in the rock, strain variations in superposed folds will greatly assist the understanding of the details of the geometry of superposed fold systems, and provide a link to the results of numerical analyses. Furthermore, as the fold shape is dependent on the lithology the interference pattern in various layers may be different because the initial folds had various stiles and amplitudes (e.g. Watkinson, 1981; Ghosh et al., 1993; Grujic 1993). Changes in interference pattern may, therefore, indicate the changes in rheology of various rock types in space and time. Potentially, when we fully understand the mechanics of active buckling of folded layers (i.e. of structurally reinforced materials) and realise numerical analyses of non-coaxial superposed folding by buckling, we may become able to extract information on the folding dynamics and on mechanical properties of rocks at various times throughout a tectonic history.

This opens the potential for future work in the study of fold interference patterns. Through analogue and numerical modelling, structural geologists should be able to: (i) provide a comprehensive kinematic model for refolding in a continuous deformation history; and (ii) develop a mechanical model for non-coaxial folding by buckling. However, regardless of their scientific importance (and

state of fashion) fold interference patterns will always maintain their aesthetic values.

### Acknowledgements

Geologisches Institut, ETH-Zurich kindly lent the models for this study. D.G. is indebted to John G. Ramsay for introducing him to the beauty of refolded folds. Constructive and detailed reviews by Chris Fergusson and Alan Whittington are gratefully acknowledged. The analyses of the data set were part of the B.Sc. thesis of T.W.; the double-scan-technique was part of the Ph.D. thesis of H.G. We thank R. Huismans for stimulating discussions.

### References

- Donath, F.A., Parker, R.B., 1964. Folds and folding. *Geological Society of America Bulletin* 75, 45–62.
- Fletcher, R.C., 1991. Three-dimensional folding of an embedded viscous layer in pure shear. *Journal of Structural Geology* 13, 87–96.
- Gärtner, H., Lehle, P., Tiziani, H.J., Volland, C., 1996. Structured light measurement by double-scan technique. In: Loffeld, O. (Ed.), *Vision Systems: Sensors, Sensor Systems, and Components*. Proceedings of SPIE 2784, pp. 21–30.
- Ghosh, S.K., 1974. Strain distribution in superposed buckling folds and the problem of reorientation of early lineations. *Tectonophysics* 21, 249–272.
- Ghosh, S.K., Ramberg, H., 1968. Buckling experiments on intersecting fold patterns. *Tectonophysics* 5, 89–105.
- Ghosh, S.K., Mandal, N., Khan, D., Deb, S.K., 1992. Modes of superposed buckling in single layers controlled by initial tightness of early folds. *Journal of Structural Geology* 14, 381–394.
- Ghosh, S.K., Mandal, N., Sengupta, S., Deb, S.K., Khan, D., 1993. Superposed buckling in multilayers. *Journal of Structural Geology* 15, 95–111.
- Grujic, D., 1993. The influence of initial fold geometry on Type 1 and Type 2 interference patterns: an experimental approach. *Journal of Structural Geology* 15, 293–307.
- Grujic, D., Mancktelow, N.S., 1995. Folds with axes parallel to the extension direction: an experimental study. *Journal of Structural Geology* 17, 279–291.
- Grujic, D., Mancktelow, N.S., 1996. Structure of the northern Maggia and Lebundin Nappes, Lepontine Alps, Switzerland. *Eclogae geologicae Helvetiae* 89, 461–504.
- Hobbs, B.E., Means, W.D., Williams, P.F., 1976. *An Outline of Structural Geology*. John Wiley and Sons, New York.
- Huber, M.I., Ramsay, J.G., Simpson, C., 1980. Deformation in the Maggia and Antigorio nappes, Lepontine Alps. *Eclogae geologicae Helvetiae* 73, 593–606.
- Johns, M.K., Mosher, S., 1996. Physical models of regional fold superposition: the role of competence contrast. *Journal of Structural Geology* 18, 475–492.
- Mancktelow, N.S., 1988. The rheology of paraffin wax and its usefulness as an analogue for rocks. *Bulletin of the Geological Institutions of the University of Uppsala N.S.* 14, 181–193.
- Mancktelow, N.S., Abbassi, M.R., 1992. Single layer buckle folding in non-linear materials—II. Comparison between theory and experiment. *Journal of Structural Geology* 14, 105–120.
- Milnes, A.G., 1974. Post-nappe folding in the western Lepontine Alps. *Eclogae geologicae Helvetiae* 67, 333–348.
- Odonne, F., Vialon, P., 1987. Hinge migration as a mechanism of superimposed folding. *Journal of Structural Geology* 9, 835–844.

- Ramsay, J.G., 1962. Interference patterns produced by the superposition of folds of similar types. *Journal of Geology* 70, 466–481.
- Ramsay, J.G., 1967. *Folding and Fracturing of Rocks*. McGraw-Hill, New York.
- Ramsay, J.G., Huber, M.I., 1987. *The techniques of modern structural geology*. Volume 2: Folds and Fractures. Academic Press, New York.
- Ramsay, J.G., Lisle, R.J., 2000. *The Techniques of Modern Structural Geology*. Volume 3: Application of Continuum Mechanics in Structural Geology. Academic Press, London.
- Skjerna, L., 1975. Experiments on superimposed buckle folding. *Tectonophysics* 27, 255–270.
- Stauffer, M.R., 1988. Fold interference structures and coaption folds. *Tectonophysics* 149, 339–343.
- Steck, A., 1998. The Maggia cross-fold: an enigmatic structure of the Lower Penninic nappes of the Lepontine Alps. *Eclogae geologicae Helvetiae* 91, 333–343.
- Tiziani, H.J., 1991. Optical methods to measure distance and topography. *Informationstechnik* 33, 5–14.
- Watkinson, A.J., 1981. Patterns of fold interference: influence of early fold shapes. *Journal of Structural Geology* 3, 19–23.
- Watkinson, A.J., Cobbold, P.R., 1981. Axial direction of folds in rocks with linear/planar fabrics. *Journal of Structural Geology* 3, 211–217.